Radar Data Processing and Visualization over Complex Terrain*

CURTIS N. JAMES, STACY R. BRODZIK, HARRY EDMON, ROBERT A. HOUZE JR., AND SANDRA E. YUTER

Department of Atmospheric Sciences, University of Washington, Seattle, Washington

(Manuscript received 19 March 1999, in final form 31 October 1999)

ABSTRACT

MountainZebra is a data flow configuration that processes and displays radar data over complex terrain. The system combines three elements: the data stream from an operational radar, 3D topographical information, and the NCAR Zebra data visualization and integration software. MountainZebra operates routinely on a 3D data stream from the National Weather Service Weather Surveillance Radar-1988 Doppler (WSR-88D) at Camano Island, Washington (near Seattle). The WSR-88D data are continuously acquired, archived, formatted, and interpolated for multidimensional display. The three-dimensional topographical information in MountainZebra can be automatically underlaid on any horizontal or vertical display of the radar data. This system allows radar data and other geophysical fields to be analyzed in precise relation to the underlying terrain.

Terrain-based visualization facilitates radar data analysis by identifying terrain clutter and shadowing and by identifying orographic precipitation mechanisms. The utility of MountainZebra is illustrated in the investigation of stable orographic enhancement over the windward slopes of the Cascade Mountains of the Pacific Northwest and an orographically enhanced squall line to the lee of the European Alps.

1. Introduction

Mountainous terrain affects radar echo patterns by interfering with the radar beam and modifying precipitation processes and patterns. When the radar beam is intercepted by terrain, clutter and shadowing result (Joss and Lee 1995; Lin and Reilly 1997). Terrain modification of the airflow affects precipitation (Smith 1979; Houze 1993, chapter 12). The spatial coverage and severity of clutter and shadowing depend on the radar characteristics, the geometry of the terrain, and the refractivity of the atmosphere, which varies with low-level stability and moisture stratification (Doviak and Zrnic 1993). In orographic regimes, the variability of the index of refraction is often greater than over flat terrain as a result of frequent low-level inversions (e.g., Gustavsson et al. 1998; Bell and Bosart 1988).

Since the 1970s, ray propagation models have been used to simulate terrain backscatter and shadowing. Recently, Lin and Reilly (1997) developed a technique that successfully reproduces terrain clutter patterns observed by shipboard radars near coastal mountains given the three-dimensional temperature and humidity of the environment and the radar characteristics and location. However, for the purpose of identifying terrain clutter and shadowing operationally, it is not necessary to quantify terrain backscatter. One needs only to overlay the 3D terrain on the 3D echo pattern at comparable spatial resolution.

Overlaying the high-resolution terrain field and the radar data (accurately located in both the horizontal and vertical) also greatly aids the physical interpretation of the radar echoes. Modification of the airflow and precipitation pattern by the topography occurs on scales ranging from individual peaks and valleys to the gross scale of the whole mountain range. Without being able to visualize precisely how the echo patterns in horizontal and vertical cross sections are juxtaposed with the topography, the analyst is handicapped.

To address these needs, we have configured a system that allows radar data and terrain to be displayed simultaneously in an operational environment. This system, called MountainZebra, consists of three elements: a data stream from an operational radar that is processed for analysis, a 3D topography database, and the National Center for Atmospheric Research's (NCAR) Zebra software (Corbet et al. 1994), which has the ability to display multiple real-time datasets. The purpose of this paper is to describe the MountainZebra system and show how the incorporation of a terrain height field into a data visualization system aids the interpretation of radar data. We first present an overview of a proof-of-concept operation of MountainZebra on real-time data from the

* Joint Institute for the Study of the Atmosphere and Ocean Contribution Number 672.

Corresponding author address: Curtis N. James, Meteorology Lab, Embry-Riddle Aeronautical University, 3200 Willow Creek Rd., Prescott AZ 86301.
E-mail: jamesc@pr.erau.edu.

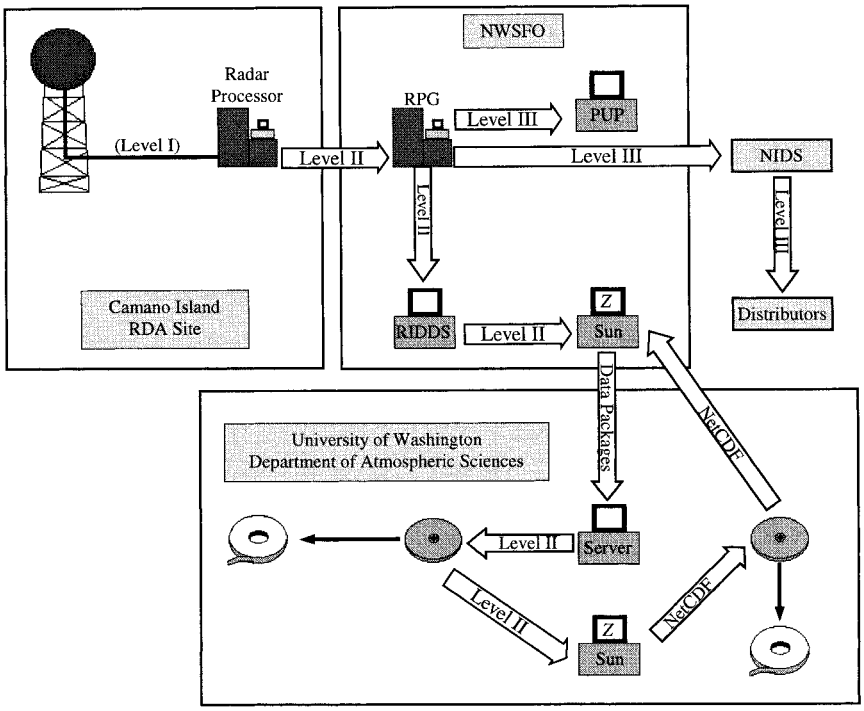

FIG. 1. Schematic of the Camano Island WSR-88D data flow. Enclosed in large rectangles are the RDA site (top left), the Seattle NWSFO (top right), and the University of Washington Department of Atmospheric Sciences (bottom). Workstations equipped with the Zebra software are indicated with a ''Z.'' Conversion to UF is not shown, but takes place at the University of Washington.

National Weather Service Weather Surveillance Radar-1988 Doppler (WSR-88D) at Camano Island, located approximately 50 km north-northwest of Seattle, Washington. Then, we illustrate the utility of superposed radar and terrain visualization in the analysis of two examples of orographic precipitation.

2. The automated data flow

Figure 1 contains a schematic of MountainZebra's automated data flow for the Camano Island radar. Raw analog radar returns (level I data) obtained by the WSR-88D propagate through the wave guide to the radar processor at the Radar Data Acquisition (RDA) site. The processor converts raw data to reflectivity, radial velocity, and spectral width in polar coordinates, applies clutter removal, and archives these data to exabyte tapes. The polar data format is hereafter referred to as level II (Crum and Alberty 1993). The level II data are then transmitted to the Radar Product Generator (RPG) at the National Weather Service Forecast Office (NWSFO), where various graphical (level III) products are produced for display at the Principal User Processor and disseminated to commercial data providers via the Next-Generation Radar (NEXRAD) Information Dissemination System. The Radar Interface and Data Distribution System (RIDDS; Rhue and Jain 1995) accesses the level II data in parallel with level III product generation within the RPG.

Via RIDDS, level II data from Camano Island go to an on-site workstation where each ray is stored in a circular buffer. Once 100 rays (i.e., 5/18 of a radar sweep) are received, they are packaged, compressed, and queued for transmission to the Department of Atmospheric Sciences at the University of Washington. The data are sent via a nondedicated communication link to the department server at rates of up to 70 kbps. The rays are then uncompressed and reassembled into full level II volumes. Each volume contains anywhere from 5 to 14 radar sweeps, depending on the volume coverage pattern (or scan strategy) used by the radar at that time. The level II volumes are written to disk, where they remain for about a week before they are archived to tape. Meanwhile, a workstation dedicated to MountainZebra processing and display immediately reads each reassembled level II volume and converts it to Universal Format [UF; Barnes (1980); this process is not shown in Fig. 1). Then, algorithms may be applied to the UF file to remove nonprecipitation echoes and correct aliased radial velocity. Finally, the data are bilinearly interpolated to a Cartesian grid using NCAR's SPRINT software (Mohr and Vaughan 1979).

Data storage limitations constrain us to use a 150 km $\times$ 150 km $\times$ 10.5 km interpolation grid with 2 km $\times$

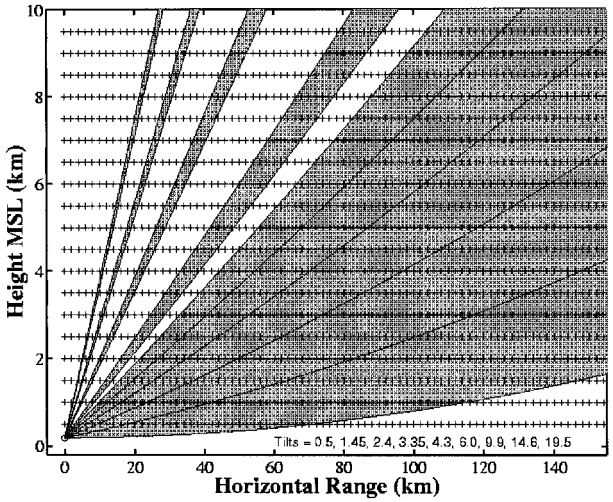

FIG. 2. WSR-88D tilt sequence using Volume Coverage Pattern 21 and assuming standard atmospheric refraction. The location of the radar dish is indicated by the open circle at 0.0-km horizontal range. The Cartesian gridpoint locations are indicated by plus signs, and the gray regions represent the cross-sectional area spanned by the radar's beamwidth.

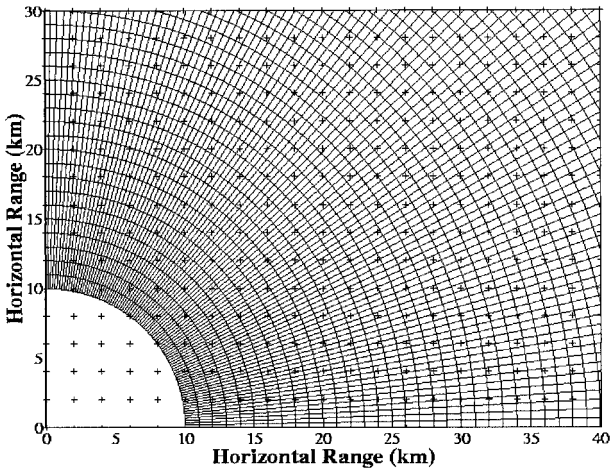

FIG. 3. The bin geometry of the northeast quadrant of the WSR-88D base reflectivity scan (0.5°) at close range, projected onto a horizontal plane. The Cartesian gridpoint locations are indicated by plus signs. The bins at range less than 10 km are not shown.

2 km resolution in the horizontal and 0.5-km resolution in the vertical. Figure 2 shows a vertical cross section of the elevation angle sequence typically employed by the Camano Island WSR-88D in precipitation mode. Figure 3 projects a small portion of the 0.5° elevation base scan onto a horizontal plane. In these figures, a 4/3 earth radius assumption[1] is used to approximate standard atmospheric refraction (Doviak and Zrnic 1993), and the Cartesian gridpoint locations after interpolation are indicated by plus signs. At low levels [<2 km above mean sea level (MSL)] and close range (<20 km), the interpolation grid reduces the vertical resolution of the tilt sequence (Fig. 2). Elsewhere, the interpolation grid is comparable to or at a finer resolution than the vertical resolution of the tilt sequence. At low levels, the WSR-88D provides 1-km resolution for reflectivity and 0.25-km resolution for radial velocity along each radial. Thus, the along-radial resolution is reduced by the 2-km horizontal interpolation everywhere in the domain. The azimuthal resolution is reduced at ranges less than 120 km, and especially at ranges less than 40 km (Fig. 3). The loss of resolution could easily be remedied by interpolating on a finer grid with the side effects of larger volume size, longer computation time for the interpolation, and greater oversampling of the grid versus the polar radar data at farther ranges. Another problem is that many of the grid points are located in data-void regions as a result of the NEXRAD scan strategy (e.g., between 4.3°, 6.0°, 9.9°, 14.6°, and 19.5° elevation scans in Fig. 2). This limitation of the scan strategy can produce concentric rings of missing data in horizontal cross sections.

Interpolating the data to a Cartesian grid facilitates the computation and display of arbitrary horizontal and vertical cross sections and makes analysis more intuitive, without the ''sawtooth'' effect seen in constant-altitude plan position indicator (CAPPI)[2] displays. The Cartesian-interpolated fields further facilitate statistical and diagnostic computations with the data, especially those that involve spatial derivatives.

After interpolation by SPRINT is complete, each volume is converted to Unidata's Network Common Data Format (NetCDF) for display. The NetCDF files are written to disk and transmitted back to the NWSFO (Fig. 1). Once the files are available on disk, dedicated workstations at both the Department of Atmospheric Sciences and the NWSFO automatically ingest the data for display. Within one to two weeks, each NetCDF volume that is deemed meteorologically significant is moved to mass storage for future reference. Radar volumes in UF format are UNIX compressed, copied to tape, and deleted from disk.

3. Terrain-based visualization in Zebra

The automated data flow, which includes the acquisition, processing, and archival of each radar volume,

[1] The current version of SPRINT makes this assumption during interpolation to approximate ray propagation. For the purpose of visually identifying terrain clutter, shadowing, and anomalous propagation, this assumption may not be adequate. Ideally, the interpolation routine should use a nearby sounding to better approximate ray propagation.

[2] CAPPI displays are traditionally produced by assigning the value of the nearest data bin in the polar-coordinate tilt sequence to each grid point of a Cartesian array. Interpolation schemes use multiple gates and multiple sweeps in the vicinity of each Cartesian grid point to estimate its value.

is finished within 2–4 min of the completion of a volume scan. MountainZebra then provides terrain-based visualization. Dedicated Zebra displays are located at both the NWSFO and the Department of Atmospheric Sciences. The displays update automatically when the processing of each new volume is complete. As described by Corbet et al. (1994), Zebra is highly interactive, allowing the user to synthesize multiple real-time datasets, overlay diverse fields, zoom in and out, specify any arbitrary horizontal or vertical cross section, change contouring options, and make time-lapse movies. MountainZebra includes topographical information on less than 1-km horizontal resolution, which can be displayed along with radar fields or other datasets in any arbitrary horizontal or vertical cross section selected by the user. Thus, four-dimensional interpretation of precipitation system structure and dynamics in relation to terrain geometry can be achieved.

The terrain contours in the horizontal and vertical cross sections were created using 30-s digital elevation data from the Defense Mapping Agency and the National Aeronautics and Space Administration, but any high-resolution elevation field on a latitude–longitude grid is acceptable. In horizontal displays, a raster image of the terrain provides a backdrop for radar and other fields. Zebra contouring options allow the foreground fields to be displayed either as color contour, filled contour, or raster plots. The extent to which the underlying terrain is visible depends on the contouring option that is used (filled contour and raster plots obscure the terrain more than contour plots).

For each vertical cross section selected by the user, a terrain profile is plotted along the horizontal axis. To achieve this terrain profile, a bilevel terrain grid was computed from the digital elevation data, with vertical levels located at 0 and 10 km and a horizontal resolution of 30 s. Each grid point was assigned the value of its altitude above ground level, with negative values indicating depth below the surface. The zero contour of this terrain grid, when bilinearly contoured in Zebra's vertical cross-section windows, produces a high-resolution terrain profile for analysis with the other fields.

There have been other attempts to overlay radar data and topography. Doick and Holt (1995) created three-dimensional displays of radar and terrain and suggested, as we do, that this would improve radar data interpretation and lead to new observational insights. MountainZebra accomplishes this goal particularly well by interpolating radar fields to a three-dimensional Cartesian grid (as opposed to vertically stacking CAPPI displays) and automatically updating. Zebra also allows the user to overlay any other relevant field (e.g., satellite data, mesoscale model fields, station data, etc.) with the radar data and terrain.

Archived radar data from other sources can also be converted to UF format, interpolated, and converted to NetCDF for analysis and display in customized versions of MountainZebra containing the appropriate topographic data. This method has been used to analyze datasets from several other radars in mountainous regions, including WSR-88D level II archives from Eureka, California, and encoded Graphical Image Format archives from the Monte Lema radar of the Swiss Meteorological Institute, near Locarno, Switzerland. The latter is part of a MountainZebra system customized for the European Alps, which was the prototype for the near-real-time system used in the 1999 Mesoscale Alpine Programme (www.joss.ucar.edu/map/).

The sample displays that follow illustrate the utility of terrain-based radar data visualization for investigating orographic precipitation. All of the radial velocity cross sections are oriented radially to facilitate interpretation. The samples include stable orographic precipitation in western Washington and a squall line to the lee of the Alps.

a. Orographic precipitation in western Washington

At 0931 UTC 23 January 1998, widespread precipitation fell over western Washington in the moist, stable flow ahead of an approaching trough. The 1200 UTC sounding taken from the coastal town of Quillayute (UIL) exhibited a freezing level of 2.3 km MSL and a stable layer that extended from 700 to 500 mb. Cross sections of Camano Island radar reflectivity (Fig. 4a) and radial velocity (Fig. 4b) at 1.5 km MSL altitude show widespread precipitation and south-southwesterly flow. Precipitation was suppressed between 80 km west and 40 km southeast of the radar site as a result of subsidence to the lee of the Olympic Mountains. Just to the northeast of this ''rain shadow,'' upslope enhancement of the precipitation was occurring over the windward slopes of the Cascade Mountains.

A vertical cross section of reflectivity (Fig. 5a) extending from the radar toward the northeast (red line segment in Figs. 4a and 4b) reveals the enhanced precipitation over the windward slopes of the Cascades. The horizontal alignment of the reflectivity contours and the enhanced reflectivity associated with a bright band between 1.5 and 3 km altitude MSL indicate that the precipitation was stratiform in nature. Orographic lifting was not destabilizing the thermodynamic profile enough to produce convection. The heaviest precipitation was occurring 50–65 km from the radar, where the reflectivity approached 40 dBZ. The radial velocity field along the same cross section (Fig. 5b) exhibited strong radial convergence in this region of maximum enhancement.

The vertical velocity w in the convergent region can be roughly estimated in two ways. Assuming incompressibility, and neglecting cross-radial divergence, the continuity equation can be approximated as

$$\Delta w \sim -\frac{\Delta u}{\Delta x}(\Delta z).$$

From Fig. 5a, we estimate that the convergence extended over an estimated 2-km depth Δz, with a deceleration

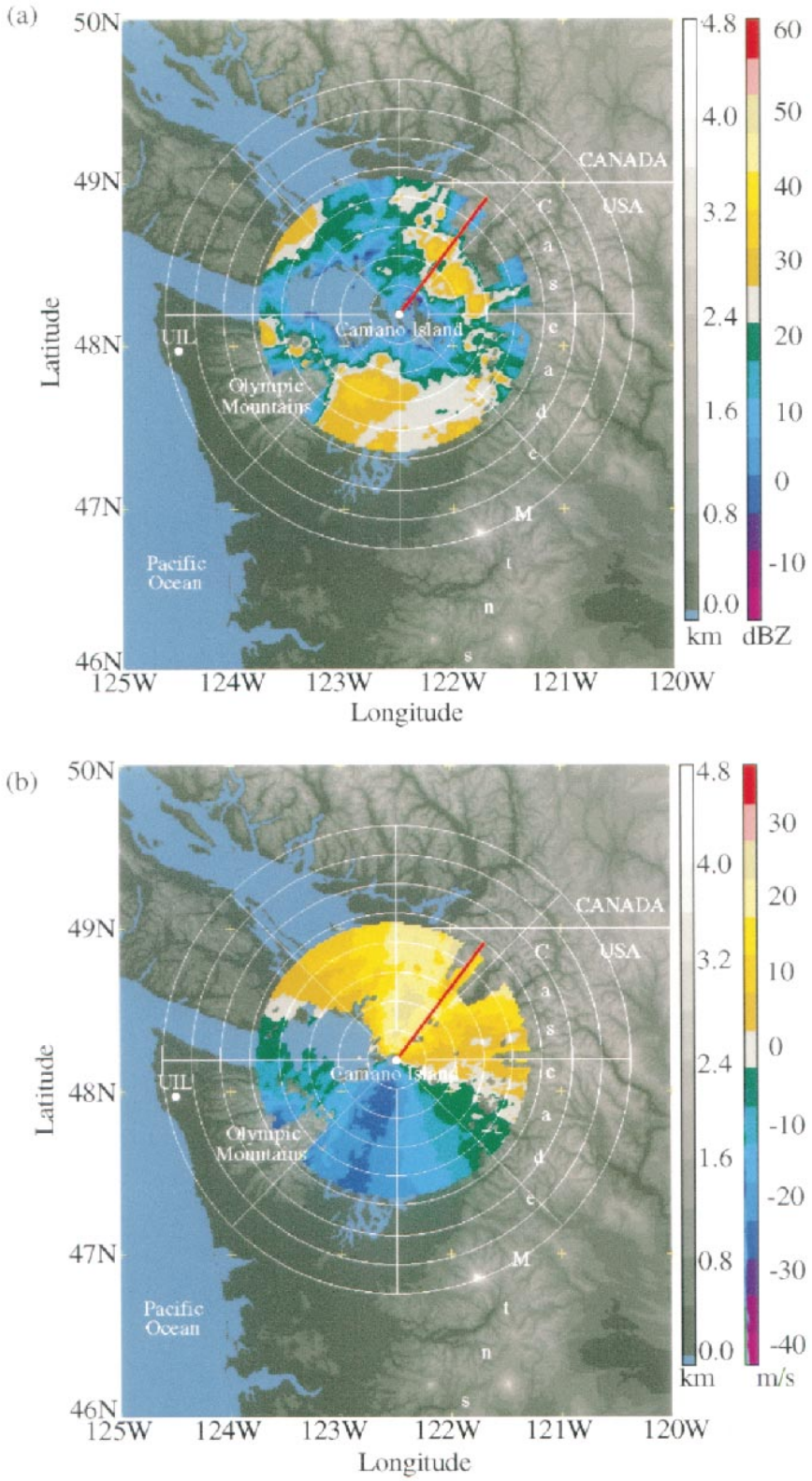

FIG. 4. Constant altitude plots at 1.5 km MSL using Camano Island WSR-88D (a) reflectivity and (b) radial velocity data from 0931 UTC 23 Jan 1998. The background topography is shown in grayscale increments of 0.4 km MSL, with altitudes ≤0.0 km shown in steel-blue. Range ring spacing is 20 km. Negative radial velocity is used to indicate inbound wind. The red line indicates the direction of the vertical cross section in Fig. 5.

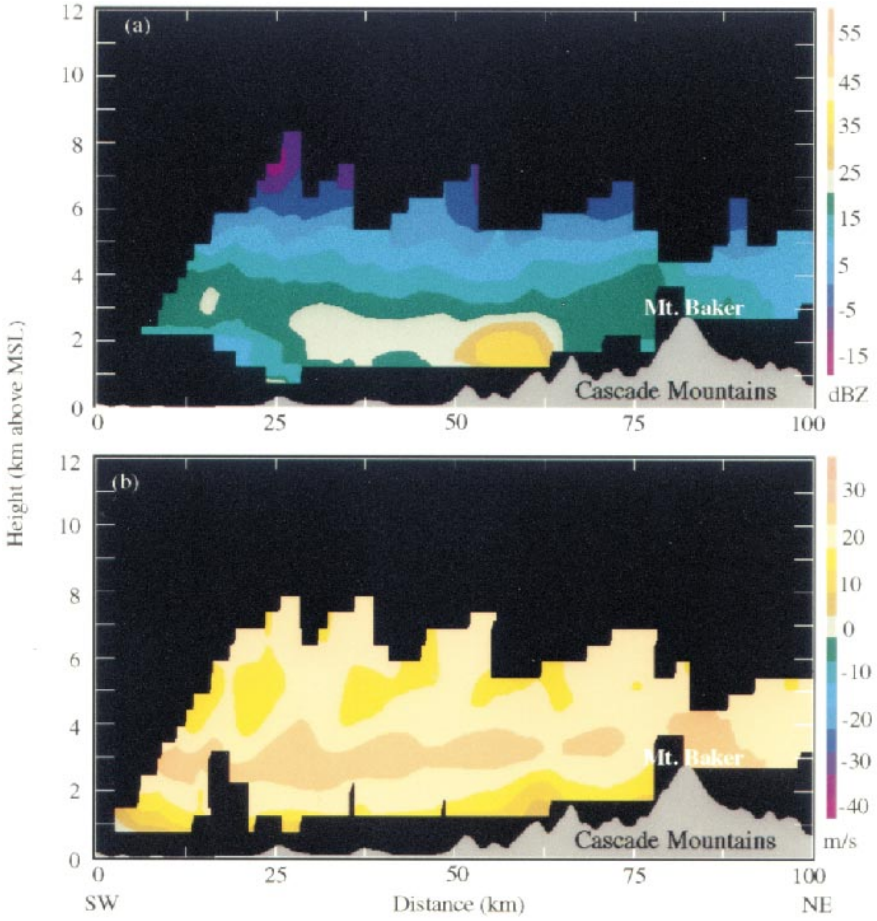

FIG. 5. Vertical cross sections of (a) reflectivity and (b) radial velocity from southwest to northeast along the red line segment in Fig. 4. The vertical profile of the underlying topography is shown in gray.

$\Delta u \sim -10$ m s^{-1} in the region $x = 50$–60 km along the cross section. Assuming that the vertical velocity at the ground was zero just upstream of the barrier, we obtain 2 m s^{-1}. Another way is to use the impermeability boundary condition for a flow U impinging on a mean slope $\Delta h/\Delta x$,

$$w \sim U\frac{\Delta h}{\Delta x}.$$

Since $U \sim 20$ m s^{-1} upstream of the barrier, and the slope 50–60 km from the radar is approximately 0.1, we obtain the same vertical velocity estimate. Thus, the radar fields are consistent with the topographical forcing.

Overlaying radar fields with the topography in vertical cross sections allowed us to identify readily where orographic enhancement was occurring. It was greatest on the lower slopes—not at the crest of the Cascade Range (which is east of Mount Baker). This characteristic was noted by Hobbs et al. (1975) in a case study of a front passing over the crest of the Cascades. Since the Camano Island radar data are being processed and archived routinely according to Fig. 1, it will be possible to determine if enhancement of the precipitation on the lower slopes is typical or just a feature of certain types of cases.

Overlaying radar volumes with topography is also advantageous when assessing data quality. In this example, we note in both Figs. 5a and 5b that the lowest scan was partially blocked by Mount Baker (the tallest peak in the terrain profile). In this region, clutter suppression has removed data where mountain slopes were exposed to the radar signals. In Mount Baker's shadow ($x = 80$ to 100 km), the returned power was less than immediately uprange.

A layer of maximum radial velocity ($\sim$25 m s^{-1}) spanned most of the vertical cross section (Fig. 5b). The radial velocity field oscillated with an apparent horizontal wavelength of 15 km. These oscillations could have been trapped internal gravity waves in the stable 700–500-mb (2.9–5.5 km) layer excited by flow over the Olympic Mountains just upstream. Although an exact quantitative assessment is not within the scope of this study, the nearest sounding available indicated a stratification that would support trapped waves. Also

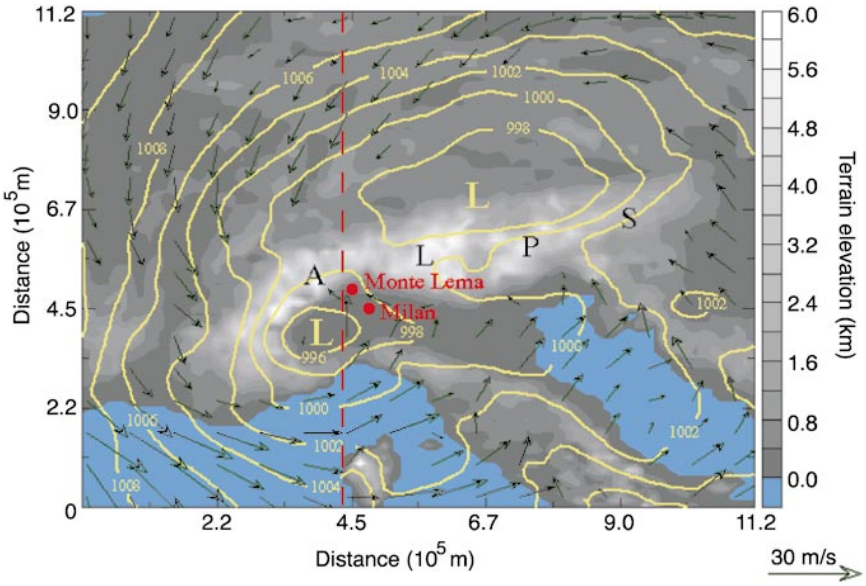

FIG. 6. The SM forecast of sea level pressure (contours) and 950-mb wind (vectors) at 0000 UTC 8 Jul 1996 (initialized 1200 UTC 7 Jul). The locations of the Monte Lema radar and Milan, Italy, are shown. The dashed red line indicates the location of the vertical profiles shown in Fig. 7.

evident in the cross section is enhanced downslope flow to the lee of Mount Baker. This enhancement was immediately evident from the topography profile that is provided in every Zebra cross section.

b. A squall line to the lee of the European Alps

On 7–8 July 1996, a squall line formed to the lee of the European Alps and was well sampled by the Swiss operational C-band Doppler radar at Monte Lema in southern Switzerland (Fig. 6). Joss et al. (1998) describe this radar system in detail. The Swiss Meteorological Institute provided us with full-volume reflectivity and radial velocity data, which were processed and interpolated to a Cartesian grid for terrain-based display. The squall line was associated with a surface mesocyclone that formed to the lee of the European Alps and then moved eastward across northern Italy under the influence of an upper-level trough. An analysis of the 14-km resolution Swiss Model (SM; Majewski 1991) simulation of this case indicates that the mesocyclone was similar to one simulated by Aebischer and Schär (1998), in terms of its location, horizontal scale, and propagation. Such lee cyclones in northern Italy are known to occur in two stages (Buzzi and Tibaldi 1978; McGinley 1982). In the first stage, the progression of a surface cold front is slowed by the terrain. Cold air invades the Mediterranean region and low-level vorticity is rapidly generated over the Gulf of Genoa and northwestern Italy. During the second stage, the rate of cyclone development decreases to that of typical baroclinic systems as the upper-level trough interacts with the low-level cyclone.

Figure 6 shows the mesoscale SM forecast of sea level pressure for 0000 UTC 8 July 1996, initialized at 1200 UTC 7 July and integrated at 12 h. The 12-h integration is commonly regarded as the best estimate of the actual meteorological conditions. By 12 h the flow has not yet deviated much from the initial conditions, but it has had time to become dynamically balanced. The balanced conditions are essential for physically consistent inferences about flow in relation to complex terrain. The SM output showed the approximate location of the mesocyclone at this time. Subsequent to 0000 UTC, the model produced northerly downslope flow (Fig. 7), with speeds of over 30 m s^{-1} by 1200 UTC.

Monte Lema radar data and terrain overlays indicated that prior to the development of downslope flow, thunderstorms were initiated by the upslope flow of moist, conditionally unstable air in the northeast quadrant of the mesocyclone. The convective activity extended from near the center of the mesocyclone toward the northeast, but exhibited very little convective organization in the weakly sheared environment. The Monte Lema radial velocity field (Fig. 8a) indicated that the downslope flow predicted by the SM converged with the flow around the mesocyclone. The convective cells intensified and became organized into a broken line (Fig. 8b), which propagated slowly to the southeast along the southeastern edge of a comma-shaped precipitation pattern in the reflectivity field (Fig. 9). The

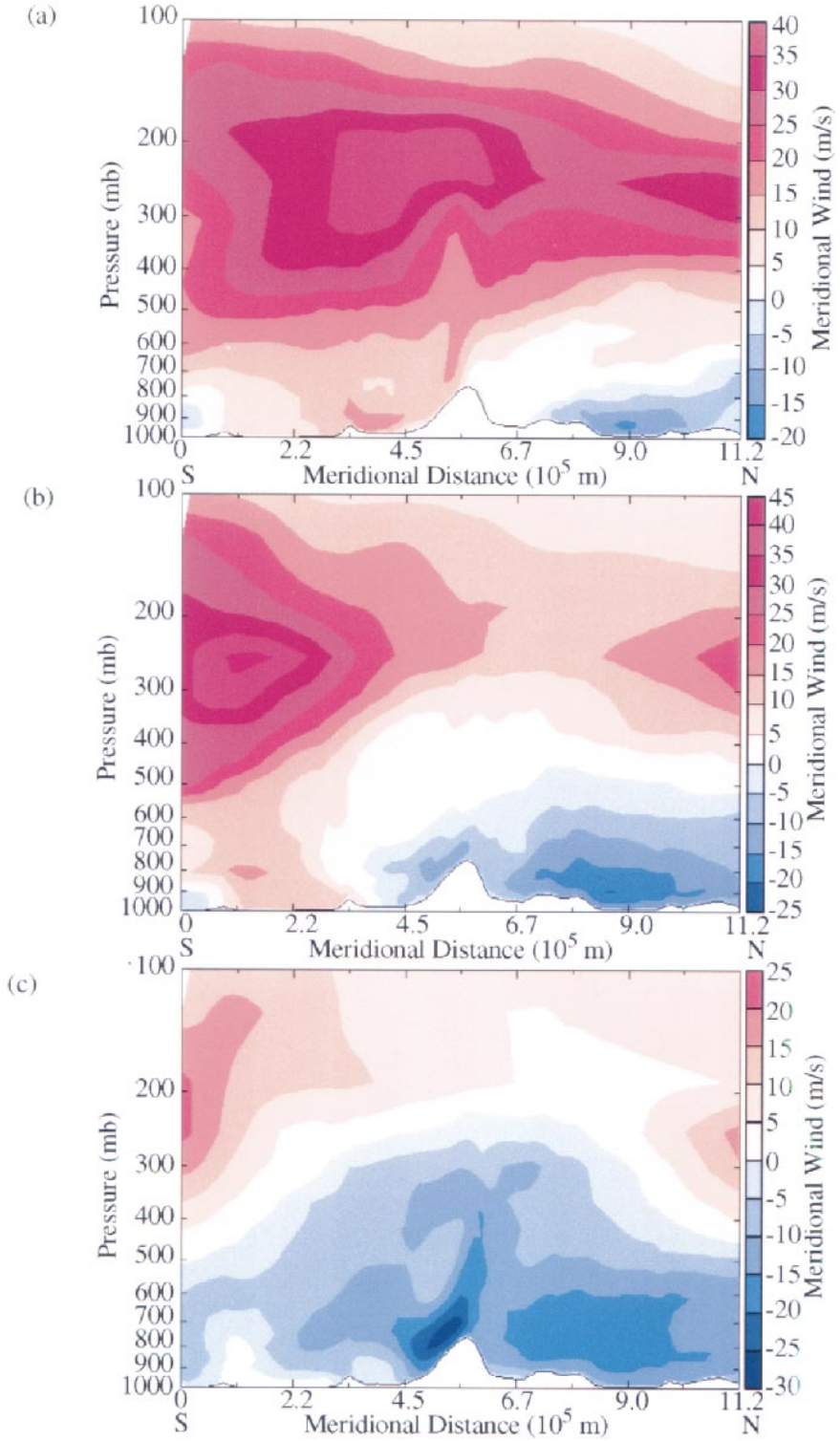

FIG. 7. Vertical cross section of the SM-simulated meridional wind along the dashed line in Fig. 6. Model fields are valid (a) 0000 UTC (initialized 1200 UTC 7 Jul), (b) 0600 UTC (initialized 0000 UTC 8 Jul), and (c) 1200 UTC 8 Jul (initialized 0000 UTC 8 Jul). Positive (negative) values indicate southerly (northerly) flow.

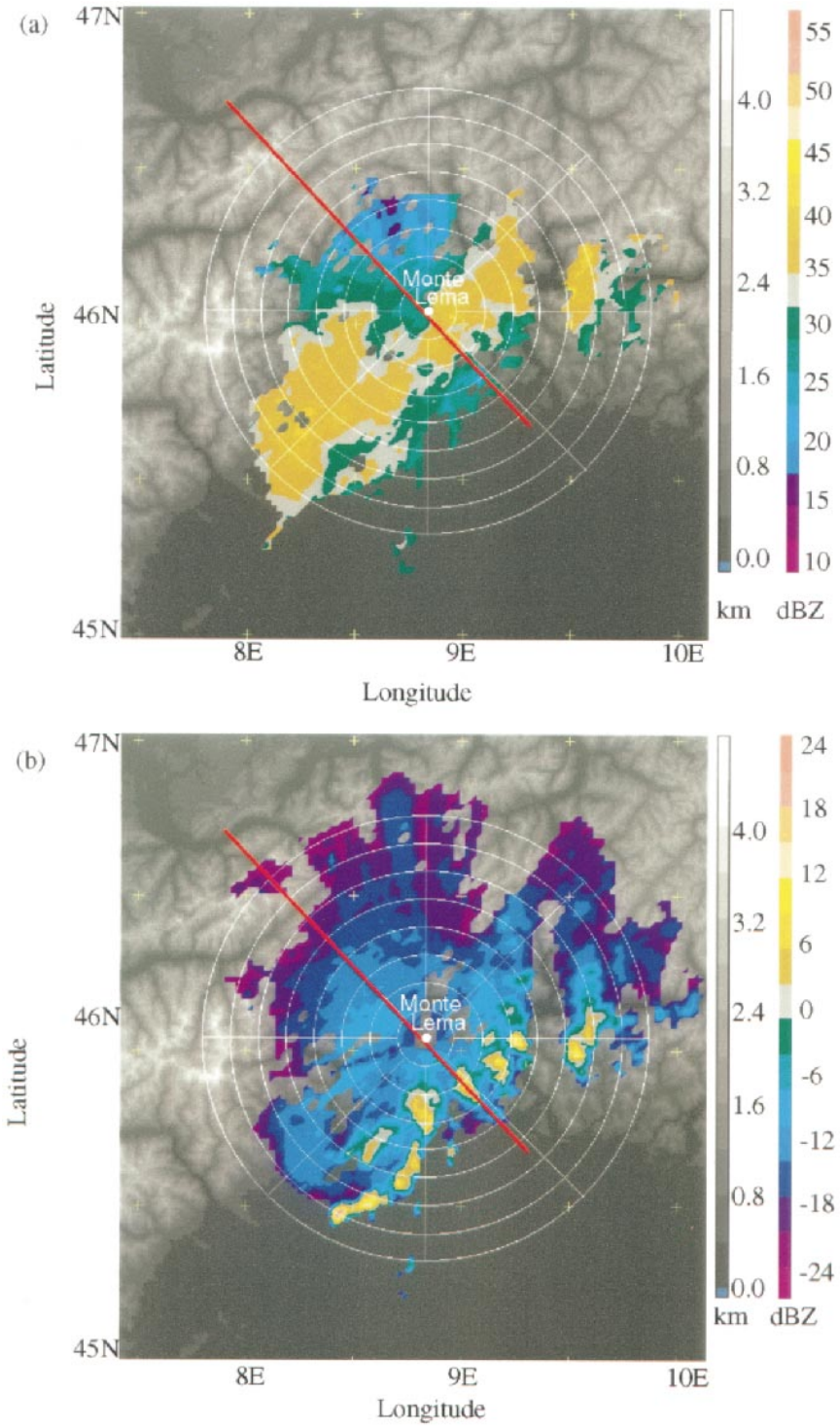

FIG. 8. MountainZebra horizontal cross sections of (a) radial velocity at 1.5 km MSL and (b) reflectivity at 3.0 km MSL from Monte Lema at 0450 UTC 8 Jul 1996. The red segment indicates the location of the vertical cross sections in Fig. 10. The range ring spacing is 10 km.

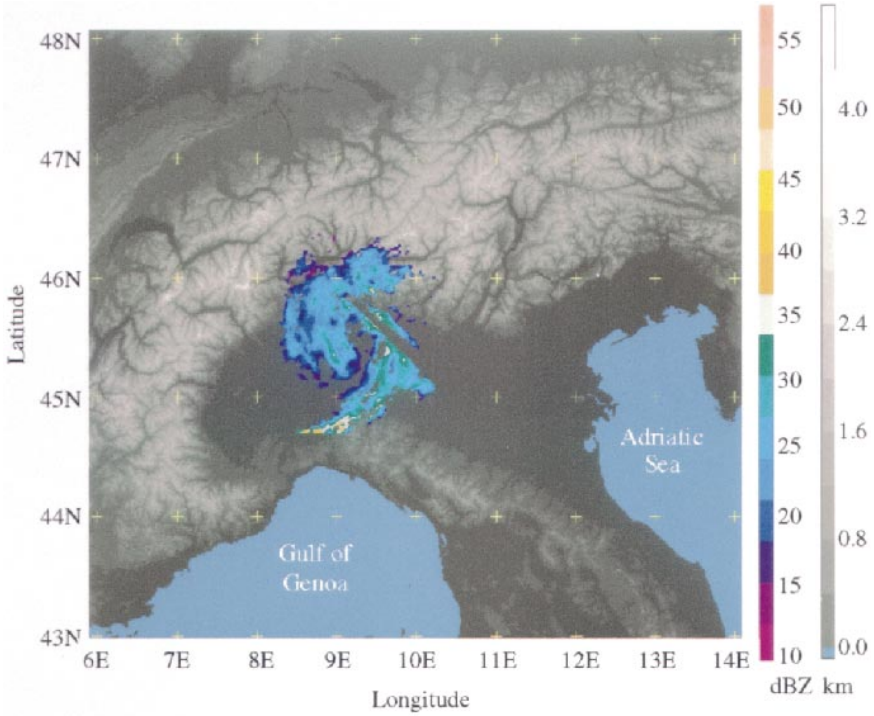

FIG. 9. MountainZebra horizontal cross section of reflectivity at 3.0 km MSL, 0750 UTC 8 Jul 1996, indicating the size and position of the lee cyclone in the context of the Alpine topography.

radial velocity field (not shown) indicated possible mesoscale rotation.

Vertical cross sections of radial velocity and reflectivity through the Alpine squall line exhibit structures that are common to midlatitude squalls (e.g., Skamarock et al. 1994). A convective cell is observed between $x = 120$ and $x = 140$ km (Fig. 10a), characterized by high reflectivity and deep vertical development. A trailing stratiform region is identified between $x = 40$ and $x = 120$ km, characterized by weaker reflectivity and horizontally aligned reflectivity contours. In the radial velocity field (Fig. 8a), there is evidence of strong low-level convergence at the base of the convective line over the foothills of the Alps ($x = 140$ km; see Fig. 10b). Other structures that can be identified are front-to-rear flow at altitudes above 6 km in the trailing stratiform region, low-level rear inflow, and evidence of strong storm-top divergence.

Despite its prototypical structure, terrain-based radar displays together with forecast model output suggest that the squall line was influenced by orography. Analysis of the evolution of the radial velocity field indicates that between 0100 and 0200 UTC, a surge of downslope flow converged with the upslope flow around the lee cyclone. It was during this time that the convection became organized into a squall line. This downslope flow was observed by radar, in radial velocity cross sections in Fig. 8a and 10b, with the most intense radial inflow immediately above the Alpine slopes. It is believed that the downslope flow enhanced the rear inflow into the squall line, contributing to its development and organization.

4. Conclusions

Terrain-based visualization improves radar data analysis over complex terrain, both in the identification of topographically induced errors and the investigation of orographic precipitation mechanisms. For this purpose, MountainZebra has been developed to acquire, process, archive, and display radar data in precise relation to the underlying terrain. Real-time WSR-88D level II data from Camano Island, Washington, are accessed via the National Severe Storm Laboratory's RIDDS system and used as input to a chain of programs that reformats and interpolates radar data for display and analysis in NCAR's Zebra data visualization system. We have included a high-resolution topography field in Zebra so that the radar data are displayed in precise relation to the terrain height in any arbitrary horizontal or vertical cross section.

The sample cases in this paper demonstrate the utility of terrain-based radar data visualization. In a stable precipitation event over western Washington, this technique aided in the identification of a rain shadow to the lee of the Olympic Mountains and stable orographic enhancement over the windward slopes of the Cascade Range. Evidence of gravity waves was also found in vertical cross sections through the radial velocity field.

Radar data from a squall line on the southern side of

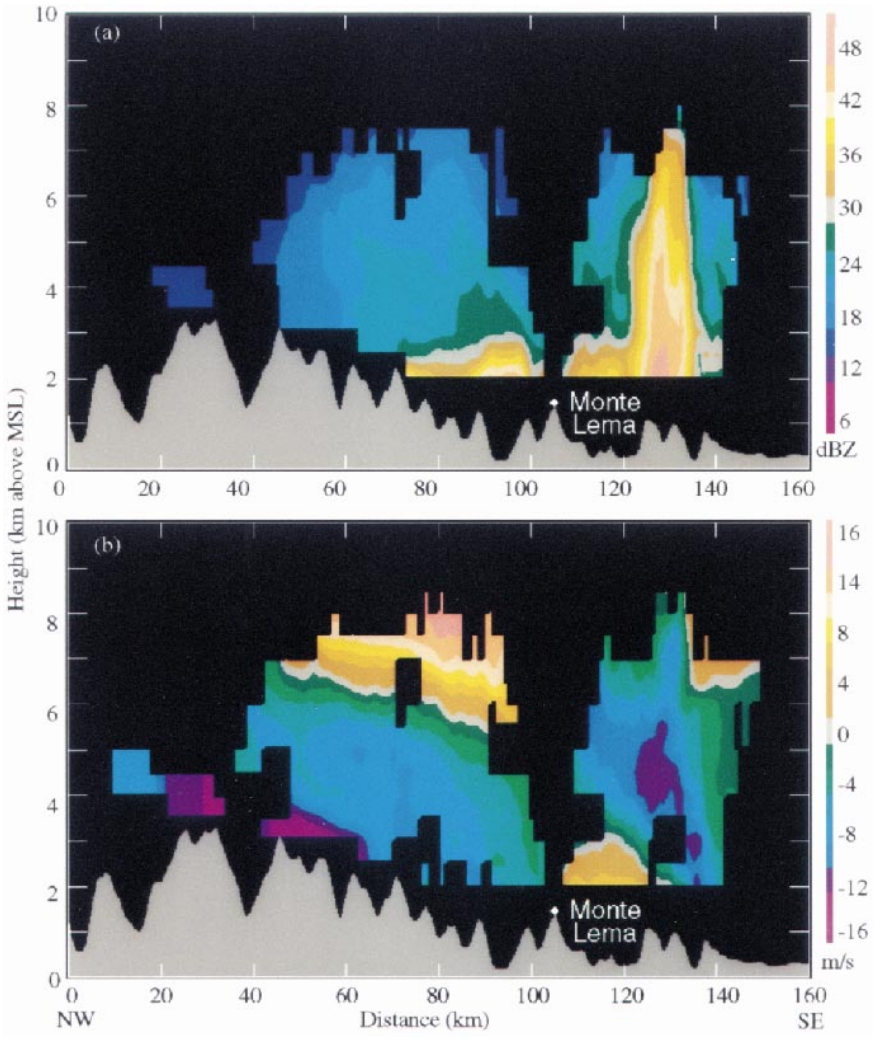

FIG. 10. MountainZebra vertical cross sections from northwest to southeast of (a) reflectivity and (b) radial velocity obtained from an interpolated 20-tilt volume scan from Monte Lema at 0452 UTC 8 Jul 1996.

the European Alps were also examined in relation to the terrain. The squall line exhibited flow structures common to midlatitude squall lines. In addition there is evidence that orographic forcing contributed to its development. Swiss Model simulations and radar observations displayed and analyzed with topography in Zebra indicate that a lee mesocyclone produced upslope flow to trigger the convection. Later, synoptically forced downslope flow converged with the flow around the mesocyclone, further contributing to the organization of the squall line.

These cases demonstrate that by interpolating radar volumes to a Cartesian grid and overlaying them with the terrain in any horizontal or vertical cross section, effective terrain-based visualization is achieved. Since Zebra can display any regularly or irregularly gridded geophysical field, this visualization technique can be expanded to include mesoscale model fields, satellite imagery, and other geophysical fields, and can be applied to both operational applications and research in mountain meteorology.

Acknowledgments. The authors appreciate the collaboration of Brad Colman and Chris Hill of the Seattle National Weather Service Forecast Office. The high-resolution terrain elevation data were provided by NCAR's Scientific Computing Division and the MAP Data Centre. Monte Lema radar data and SM fields were provided by Jürg Joss, Gianmario Galli, and Peter Binder of the Swiss Meteorological Institute. Candace Gudmundson edited the manuscript. This research was supported in part by National Science Foundation Grant ATM-9409988, Office of Naval Research Grant N00014-97-0717, National Aeronautics and Space Administration Grant NAG5-1599, and by JISAO Cooperative Agreement NA67RJ0155.

REFERENCES

Aebischer, U., and C. Schär, 1998: Low-level potential vorticity and cyclogenesis to the lee of the Alps. *J. Atmos. Sci.,* **55,** 186–207.

Barnes, S. L., 1980: Report on a meeting to establish a common Doppler radar data exchange format. *Bull. Amer. Meteor. Soc.,* **61,** 1401–1404.

Bell, G. D., and L. F. Bosart, 1988: Appalachian cold air damming. *Mon. Wea. Rev.,* **116,** 137–161.

Buzzi, A., and A. Tibaldi, 1978: Cyclogenesis in the lee of the Alps: A case study. *Quart. J. Roy. Meteor. Soc.,* **104,** 271–287.

Corbet, J., C. Mueller, C. Burghart, K. Gould, and G. Granger, 1994: Zeb: Software for integration, display, and management of diverse environmental datasets. *Bull. Amer. Meteor. Soc.,* **75,** 783–792.

Crum, T. D., and R. L. Alberty, 1993: Recording, archiving, and using WSR-88D data. *Bull. Amer. Meteor. Soc.,* **74,** 645–653.

Doick, J. J., and A. R. Holt, 1995: Combined three-dimensional displays of weather radar data with terrain. Preprints, *27th Conf. on Radar Meteorology,* Vail, CO, Amer. Meteor. Soc., 371–372.

Doviak, R. J., and D. S. Zrnic, 1993: *Doppler Radar and Weather Observations.* 2d ed. Academic Press, 562 pp.

Gustavsson, T., M. Karlsson, J. Bogren, and S. Lindqvist, 1998: Development of temperature patterns during clear nights. *J. Appl. Meteor.,* **37,** 559–571.

Hobbs, P. V., R. A. Houze Jr., and T. J. Matejka, 1975: Dynamical and microphysical structure of an occluded frontal system and its modification by orography. *J. Atmos. Sci.,* **32,** 1542–1562.

Houze, R. A., Jr., 1993: *Cloud Dynamics.* Academic Press, 573 pp.

Joss, J., and L. Lee, 1995: The application of radar–gauge comparisons to operational precipitation profile corrections. *J. Appl. Meteor.,* **34,** 2612–2630.

——, and Coauthors, 1998: Operational use of radar for precipitation measurements in Switzerland. Final Rep. NRP 31, ETH Zürich, Zürich, Switzerland, 108 pp.

Lin, C. C., and J. P. Reilly, 1997: A site-specific model of radar terrain backscatter and shadowing. *Johns Hopkins APL Tech. Dig.,* **18,** 432–447.

Majewski, D., 1991: The Europa-Modell of the Deutscher Wetterdienst. *Proc. ECMWF Seminar on Numerical Methods in Atmospheric Models,* Vol. 2, Reading, United Kingdom, European Centre for Medium-Range Weather Forecasts, 147–191.

McGinley, J., 1982: A diagnosis of Alpine lee cyclogenesis. *Mon. Wea. Rev.,* **110,** 1271–1287.

Mohr, C. G., and R. L. Vaughan, 1979: An economical procedure for Cartesian interpolation and display of reflectivity factor data in three-dimensional space. *J. Appl. Meteor.,* **18,** 661–670.

Rhue, D. T., and M. H. Jain, 1995: A RISC-based WSR-88D interface and workstation. Preprints, *11th Int. Conf. on Interactive Information and Processing Systems for Meteorology, Oceanography, and Hydrology,* Dallas, TX, Amer. Meteor. Soc., 235–239.

Skamarock, W. C., M. L. Weisman, and J. B. Klemp, 1994: Three-dimensional evolution of simulated long-lived squall lines. *J. Atmos. Sci.,* **51,** 2563–2584.

Smith, R. B., 1979: Influence of mountains on the atmosphere. *Advances in Geophysics,* Vol. 21, Academic Press, 87–230.